CLM-P656

UKAEA

Preprint

COMPUTERISED TOMOGRAPHY FOR SPARSE-DATA PLASMA PHYSICS EXPERIMENTS

J. H. WILLIAMSON
D. E. EVANS

CULHAM LABORATORY
Abingdon Oxfordshire

1982

CLM-P 656

COMPUTERISED TOMOGRAPHY FOR SPARSE-DATA PLASMA PHYSICS EXPERIMENTS

Report on JET Design Study Contract B-EH-440

J H Williamson* and D E Evans

Culham Laboratory, Abingdon, Oxon OX14 3DB, England
(Euratom/UKAEA Fusion Association)

A B S T R A C T

Matrix inversion and least squares fitting have been used to recover two-dimensional distribution functions from a small number of line integrals taken along chords across them. A self-consistent optimization procedure, free from reliance on comparison with a trial source function, for optimizing the configuration of these chords is described and used to demonstrate that an asymmetric arrangement usually leads to greater reconstruction accuracy than a regular array.

Smoothing is incorporated by imposing auxiliary conditions relating to the second derivative $\nabla^2 f$ of the source function f, and its effect on reconstruction accuracy and resolution is investigated.

These methods are applied to the ten-channel far-infrared interferometer being prepared for use on JET. Electron density contour shapes can be identified rather sensitively if the source function contours belong to a predetermined family.

(Accepted for publication in IEEE Trans. Plasma Science)

September 1981

*Modes Scientific Consultancy Ltd 73-75 George St Oxford

1. INTRODUCTION

Many plasma diagnostics measure line integrals of quantities such as electron density, Faraday rotation, electron cyclotron emission, visible, ultra-violet, and x-ray emission. In a plasma whose cross-section is circularly symmetric, the two dimensional distribution corresponding to these line integral projections is routinely recovered by the use of the Abel transform [1]. For more complicated cross-sections having higher order symmetry or no symmetry at all, such as the ellipse and the quasi-D shapes expected in the next generation of experiments on magnetically confined plasma (JET,TFTR) the local quantities can better be reconstituted by methods of computerised tomography [2].

These methods have already been extensively exploited in medical radiography [3] and in radio astronomy [4], but their potential in fusion research diagnostics is only beginning to be appreciated [5].

The general problem can be formulated by reference to Figure 1, where f(x,y) is a two-dimensional distribution of some property in a plasma. Let

$$h = -x \sin\theta + y \cos\theta$$

be a straight line whose perpendicular distance from the origin is h, θ being the angle between the line and the x-axis. The integral along this line is

$$I(\theta,h) = \int_{-\infty}^{\infty}\int f(x,y)\ \delta(-x \sin\theta + y \cos\theta - h)\ dx\ dy \qquad \ldots(1)$$

$\delta(\ )$ being the Dirac δ-function. The problem is to invert the integral to obtain an explicit expression for f(x,y), given $I(\theta,h)$.

The solution to this problem was first found and its uniqueness demonstrated by J Radon in 1917 [6]. A M Cormack analysed the problem in terms of an expansion in circular harmonics [7], giving

integral equations analogous to the Abel equation. Bracewell [4] showed that line integrals of the above type are related to the Fourier transform of $f(x,y)$, and by Fourier techniques deduced the inversion

$$I(h,\theta) \xrightarrow{F_1} \underset{\text{polar}}{S(k,\theta)} = \underset{\text{cartesian}}{S(k_x,k_y)} \xrightarrow{F_2} f(x,y) \qquad \ldots(2)$$

where F_1 and F_2 mean single and double Fourier transforms respectively.

Williamson and Clarke [8] and others extended the analysis to three dimensions, and further advances have now been made by many investigators, e.g. [9].

The problem addressed by computerised tomography is the identification of a suitable numerical technique corresponding to the above sort of analytical inversion, and a review of techniques in current use in radiology is provided by Budinger and Gullberg [2]. The plasma diagnostics problem differs from the radiological one in two respects. In the first place, in contrast, say, to the EMI scanner, $I(\theta,h)$ may be known at only a few points, possibly less than 100, and perhaps even less than 10, so methods like filtered back projection may be quite inappropriate. The second difference is that the plasma often does present some symmetry, and knowledge of that can greatly simplify the reconstruction.

In this paper, Section 2 describes our basic method, and following Sections discuss the choice of the best experimental configuration, and the questions of smoothing and resolution. In Section 6 we apply our results to an example with very few lines of sight, submillimetre interferometry of magnetically

confined plasma [10], making explicit use of the symmetry. Section 7 considers the optimal design of an experiment on a square mesh, and Section 8 deals with an example of a larger number of sight lines as in bolometry or spectroscopy.

2. THE PROBLEM AND ITS SOLUTION

The distinctive feature of the problem in plasma physics experiments is the restriction to a small number of lines of sight, and the principal question is how to optimise their use. In the absence of any further information, one would have to divide the plasma cross-section into an array of J pixels, Figure 2(a), and the signals observed along L lines of sight traversing the array would be

$$I_\ell = \sum_j A_{\ell j} f_j \qquad \ldots(3)$$

where the matrix elements $A_{\ell j}$ represent the extent that the source function f_j in pixel j contributes to the signal on line ℓ. Straightforward matrix inversion then allows us to find f_j. The number of resolved pixels would be at most the number of lines of sight, L ,and because L is small, little plasma structure would be revealed by such a procedure.

We have therefore assumed that the shape of the contours of the distribution under investigation (say density) is known, for instance because they coincide with magnetic surface contours. The pixels might then be defined as lying between pairs of such contours, Figure 2(b).

A particular choice of J pixels and of L lines of sight, each of the latter determined by its co-ordinates (θ,h), allows the components of the L x J matrix $A_{\ell j}$ specific to that choice to be evaluated. At its simplest, $A_{\ell j}$ could be taken to be the

length of the line ℓ inside the pixel j. The more accurate definition for $A_{\ell j}$ actually adopted in our computation is discussed in the Appendix.

In general the number of lines of sight L is different from the number of pixels J, so a least squares fitting [11,14] is used. This means that the quantity

$$\chi^2 = \sum w_{m\ell}(I_\ell - \sum_j A_{\ell j} f_j)(I_m - \sum_j A_{mj} f_j) \qquad ...(4)$$

is minimised. Here, $w_{m\ell} \equiv [\mathrm{covar}(I_m, I_\ell)]^{-1}$ is a weighting function. In what follows, for simplicity of presentation, we will regard actual measurements as statistically independent, so the weighting matrix w is taken to be diagonal with zero off-axis elements, and $w_{\ell\ell} = \frac{1}{\mathrm{var}(I_\ell)} \equiv w_\ell$.

Before matrix inversion can be performed, a square symmetric, positive definite matrix Q is constructed from the product of matrix A and its transpose A^T:

$$Q_{jk} = \sum_{m,\ell} A^T{}_{jm}\, w_{m\ell}\, A_{\ell k} \,. \qquad ...(5)$$

If the number of lines of sight L is fewer than the number of pixels J, viz $L<J$, then $\det Q = 0$, and matrix inversion is impossible. But for $L \geq J$, Q can be inverted and the source function f_j calculated from

$$f_j = \sum_{m,\ell} \Big[\sum_k Q^{-1}_{jk}\, A^T_{km}\, w_{m\ell} \Big] I_\ell \equiv \sum_\ell M_{j\ell}\, I_\ell \,. \qquad ...(6)$$

The matrix $M \equiv Q^{-1} A^T w$ characterises a particular choice of lines of sight and pixels, and it is stored and used to compute f_j's from the observed I_ℓ's measured in this particular configuration. The accuracy of the reconstruction is given by the $\mathrm{covar}(f_j, f_k) = Q^{-1}_{jk}$.

3. OPTIMISING THE CONFIGURATION OF LINES OF SIGHT

(a) For guidance in optimising the configuration of lines of sight, we have invented a quantitative measure of the freedom from redundancy, or "usefulness", u_ℓ, of any line of sight ℓ. The configuration can be varied and u_ℓ calculated for all the lines for each variation. An optimum configuration is that for which the minimum u_ℓ is maximised.

The concept of "usefulness" has emerged from the following considerations. Suppose a measurement were performed on all lines of sight except the line $\ell=1$. It might prove possible to calculate a value for the signal on $\ell=1$ via equations 6 and 3, from the measured values of the signals on all the other lines of sight $\ell=2,3,\ldots L$. This calculated value for the signal on $\ell=1$, call it I_1^C, would have an associated variance, call it $\mathrm{var}(I_1^C) \equiv 1/ w_1^C$, which would be calculated from the measured variances on $I_2, I_3 \ldots I_L$.

Now suppose the signal on the line of sight $\ell=1$ is actually measured, resulting in I_1 and $\mathrm{var}(I_1) \equiv 1/ w_1$. Then the best estimate for the value to be associated with the line $\ell=1$ must be the mean of the measured value I_1 and its calculated counterpart I_1^C, weighted according to their respective variances, viz

$$I_1^e = \frac{w_1 I_1 + w_1^C I_1^C}{w_1 + w_1^C}$$

and having a variance $\mathrm{var}(I_1^e) \equiv \dfrac{1}{w_1^e}$ where $w_1^e = w_1 + w_1^C$.

If I_1^C is only weakly dependent on $I_2, I_3, \ldots I_L$, then $\mathrm{var}(I_1^C)$ will be large; the best estimate $I_1^e \sim I_1$, and $w_1^e \sim w_1$. Since the signal on $\ell=1$ can be calculated only inadequately from the measured signals on $\ell = 2, 3, \ldots, L$, the measured signal

I_1 on $\ell=1$ contributes mainly non-redundant information to the best estimate I_1^e , and it can therefore be regarded as a "useful" measurement.

On the other hand, if the calculated value I_1^c is a good estimate for I_1, then the var (I_1^c) will be small, meaning $I_1^e \sim I_1^c$, and var $(I_1^e) \sim$ var (I_1^c) . Since the signal on $\ell=1$ can now be calculated very satisfactorily from the measured signals on I_2 $I_3,\ldots,I_L$, the measured signal on $\ell=1$ contributes mainly redundant information to the best estimate I_1^e , and it can therefore be thought of as a "not useful" measurement.

As a quantitative measure of usefulness u_ℓ to be attached to a particular line of sight, we have accordingly adopted the normalised variance

$$\begin{aligned} u_\ell &\equiv \text{var}(I_\ell^e)\, w_\ell \\ &= \sum_{j,k} A_{\ell j}\, \text{covar}(f_j, f_k)\, A^T_{k\ell}\, w_\ell \qquad \ldots(7) \\ &= \sum_{j,k} A_{\ell j}\, Q^{-1}_{jk}\, A^T_{k\ell}\, w_\ell \ . \end{aligned}$$

The values of the normalised variance u_ℓ calculated according to the foregoing recipe from the basic matrix A of the configuration lie in the range 0 to 1. If $u_\ell < 1$, it means that the measurement ℓ is partly redundant in that the information it conveys is already partly available from the rest of the lines of sight. If $u_\ell = 1$, its information is completely fresh. By varying the values of θ and h defining a line, its usefulness can be varied, and one seeks that configuration for which the minimum value of u_ℓ is maximised.

An important property of the usefulness parameter u_ℓ is that its sum over all the lines of sight is invariant (but see

Section 4 below) and equal to J , the number of pixels.

$$U \equiv \sum_{\ell} u_{\ell} = \sum_{\ell}\Big[\sum_{j,k} A_{\ell j}\, Q^{-1}_{jk}\, A^{T}_{k\ell}\Big]\, w_{\ell} = \sum_{j,k} Q^{-1}_{jk}\Big[\sum_{\ell} A^{T}_{k\ell}\, w_{\ell}\, A_{\ell j}\Big]$$

$$= \sum_{j,k} Q^{-1}_{jk}\, Q_{jk} = \sum_{j} \delta_{jj} = J \,. \qquad \ldots(8)$$

(b) An alternative guide to the optimum configuration is furnished by the sum of the errors on the f_j's resulting from their reconstruction from the measured set of I_ℓ's and their variances. This quantity is the trace of the matrix Q^{-1}:

$$T \equiv \sum_{j} \mathrm{var}(f_j) = \sum_{j} Q^{-1}_{jj} \qquad \ldots(9)$$

and the optimum configuration would be identified as that for which T is a minimum.

In contrast to the method advocated by Frieder and Herman [15] who measure the success of their reconstruction by comparing with the original source distribution, our approach relies entirely on self-consistency of the data, and makes no appeal to any particular test distribution.

4. SMOOTHING

Data is sparse and it behoves us to utilize all the information at our disposal in attempting to deduce the source function f . And we do indeed know more about f than what is conveyed by a set of measurements along the lines of sight. For example, we know the plasma is inside and not outside the vessel; we know it has zero density at some boundary, and that it varies fairly smoothly within the boundary. It would be unnecessarily self-denying to ignore this information in

reconstructing f , and we therefore choose to adopt a Bayesian approach and introduce this a priori knowledge through a technique of smoothing the measured data.

Without smoothing, the set of equations that are to be solved for the f_j's would be ill-conditioned, all the $A_{\ell j}$'s being positive, and the resulting uncertainties attached to the f_j's would actually turn out to be larger than one might have expected in view of the accuracy of the measurements on the chords.

The errors on the f_j's could be reduced by decreasing the number of pixels relative to the number of chords so that we would deal in effect with an overdetermined set. For example, Sweeney and Vest [14] with 102 sight lines retained only 36 of their extended basis functions (their analogue to our pixels) to diminish their reconstruction error.

Such a strategy is ruled out for us by our aim of being able to deal with an interferometer having only 10 sight lines. Instead, we choose to reduce reconstruction errors by introducing smoothing, which has the effect of relaxing the restriction that the number of pixels must be less than or equal to the number of lines of sight. This means that a more accurate calculation of the $A_{\ell j}$ coefficients is possible, and also the optimization of the location of the chords is not artificially dependent on the exact arrangement of the pixels.

One way to introduce smoothing is to impose auxiliary conditions relating to the second derivative $\nabla^2 f$ of the source function. Setting $\nabla^2 f = 0$ would imply f uniformly zero, while $\nabla^2 f =$ constant implies some knowledge of the absolute magnitude of f. However, the choice of $\nabla^2 f = - K^2 f$ gives a "consistent" result when the constant of proportionality, $-K^2$, is the smallest eigenvalue of the operator ∇^2. By this we mean that if a measurement were made on only one line of sight, we could expect to deduce only a single datum from it, namely a scaling factor, while the shape of the distribution f would be entirely determined by the smoothing conditions. For instance, in the case of circularly symmetric pixels, the profile would be the zero order Bessel function $J_o(Kr)$ with its first zero at the boundary.

Smoothing is incorporated into the calculation by extending the set of equations (3), by adding further members of the form

$$0 = \beta \Sigma (\nabla^2 + K^2) f_j \equiv \beta \Sigma B_{mj} f_j \qquad \ldots(10)$$

where the arbitrary constant β determines the amount of smoothing.

We now do the least squares fit to the new extended set of equations

$$\begin{aligned} I_\ell &= \sum_j A_{\ell j} f_j \\ 0 &= \sum_j \beta B_{mj} f_j \ . \end{aligned} \qquad \ldots(11)$$

Hitherto the usefulness parameter was attached to each line of sight, and it was shown that the sum of u_ℓ over all lines of sight resulted in a constant value J, the number of pixels into which the source function is divided. A natural extension of the idea of usefulness to embrace smoothing is secured by attaching the usefulness parameter not so much to the physical line of sight as to the individual equations in the set (11). The first L of these indeed do stand for lines of sight, but the rest are auxiliary smoothing equations. By going through an argument analogous to that leading to equation (8), it is readily shown that the sum of the extended usefulness parameters, summed over not only lines of sight but all the equations in set (11), remain equal to J, the number of pixels. Thus in the presence of smoothing, the usefulness in its extended definition, summed over lines of sight only, must be less than J.

So smoothing diminishes the usefulness of the lines of sight, thus too much smoothing is undesirable because in the limit of large β, the f_j's will have been reconstructed almost wholly on the basis of artificial smoothing. At the same time, non-zero β can be seen to reduce the uncertainty of the f_j's. That is, $T \equiv \Sigma \text{ var}(f_j)$ is reduced.

When $\beta \sim 0$, with $L = J$, all lines of sight are nearly as useful as they are ever going to be, and the total usefulness is saturating, then only T can be used as a guide to optimising the configuration. When there are more lines than pixels ($L > J$) or when we have smoothing ($\beta > 0$) there is scope for

optimising the configuration using the minimum usefulness. In practice we have usually found that minimising T is the more effective procedure. Over a sequence of a few tens of attempts to optimise a design, a better minimum u_ℓ was achieved by working with T , than by trying to increase the minimum u_ℓ directly. Increasing the minimum u_ℓ seems as likely to lead to a higher as to a lower value of T, whereas when minimising T the minimum u_ℓ seems either to increase or remains more or less unchanged, but it seems never to decrease much. This effect may result from concentrating on one line, that for which u_ℓ is minimum, when trying to increase the minimum u_ℓ directly, even though a change elsewhere, better reflected in the value of T, can have overall a more beneficial effect.

We are left with the question of the best level for the smoothing, and one possible criterion is suggested by a consideration of resolution.

5. RESOLUTION

Each measurement along line of sight ℓ results in a definite datum I_ℓ , and I_ℓ is the sum of positive contributions from all the pixels through which the line ℓ passes. If in reconstructing the f_j's one decides that the contribution to I_ℓ from one pixel should be larger, say, then the contribution to I_ℓ from its neighbour must ipso facto be smaller: there is a natural negative covariance Q^{-1}_{jk} between adjacent pixels j and k .

Incorporating smoothing tends to compensate for these negative covariances and too much smoothing results in the Q^{-1}_{jk}'s becoming positive, which can be regarded as unnatural. This amounts to saying that smoothing has smeared out the pixels to such a degree that adjacent ones are no longer distinct, and the resolution

has thereby been diminished. We therefore increase smoothing only until $Q^{-1}_{jk} = 0$, at which point adjacent pixels j and k can be said to be marginally resolved.

The meaning to be attached to the phrase "resolution of adjacent pixels" is clear when the pixels form a nested set based on magnetic field contours. But the concept demands further interpretation in the case of a pixel array in two dimensions, such as a square array. The idea here is illustrated by reference to Figure 3(a), which shows dots at the centre of each pixel in a square array of 25 elements, traversed by a small number ,6, of randomly placed lines of sight. In Figure 3(b) the pixel centres are joined by lines, solid where the pair of pixels exhibit positive correlation ($Q^{-1}_{jk}>0$) and dotted when they exhibit negative ($Q^{-1}_{jk}<0$). Though it need not have turned out so, in this particular example, there is a solid line route directly or indirectly,between every pair of pixels. Even though there exist some negative correlations shown by the dotted lines, the set of all pixels constitutes a single, unresolved whole. On the scale of the pixel separation distance, then, this array shows no resolution.

We next increase the inspection scale length by discarding alternate pixels, as has been done in Figure 3(c), where lines joining the surviving pixels are now diagonal. The values of Q^{-1}_{jk} are again examined for all pairs, and the results shown by the lines are that three pixels, being negatively correlated with all their neighbours, are individually resolved, and a fourth group comprising the ten remaining pixels is one unresolved smear. This group of ten is processed still further with the result shown in Figure 3(d). In fact no further pixels have been resolved at this stage. Further discarding of alternate pixels

and recalculating of Q_{jk}^{-1}'s leads, through Figure 3 (e) to the final result Figure 3(f) where at last five pixels have been completely resolved from each other. The lines in the last Figure are a rough delineation of the boundaries of each resolved region and show the pattern of resolved areas characteristic of the particular configuration of six lines of sight with which we started. Superimposing Figure 3(a) upon 3(f) shows that the lines of sight lie near the boundaries of the resolved regions. As no line of sight happened to traverse the lower right hand quadrant, it is perhaps not surprising that this whole area remained unresolved.

6. APPLICATION OF THE METHOD TO TOKAMAK INTERFEROMETRY

(a) Interferometry at 195 μm wavelength is designed to measure the electron density distribution in the JET tokamak where densities in the neighbourhood of $10^{13} cm^{-3}$ are anticipated. Engineering constraints impose severe limitations on the number and location of possible lines of sight, and we investigated configurations consisting of seven vertical and three oblique lines arranged to fit into the ports available. The exact positions of the vertical lines of sight were fixed, but limited freedom, particularly with respect to angle was allowed to the oblique lines, which will be reflected back on themselves by mirrors, and thus will traverse the plasma twice.

The electron density distribution was assumed to possess the same symmetry as the magnetic contours, which in JET can vary through ellipses and circles to D-shapes, as described by Green et al [12]. The pixels were accordingly chosen to be a set of nested annuli centred on magnetic contour lines. The particular choice of contours used throughout this investigation

were those described in the Appendix as JET standard. They are illustrated in Figure 4.

Twenty pixels were chosen, first because the more pixels, the less their choice influences the configuration of lines of sight, and second because the spatial resolution is more readily determined with many pixels. The pixels were spaced according to ψ (see Appendix) rather than for instance $\sqrt{\psi}$ or ψ^2, and this gave them approximately equal areas. It also meant they were more closely spaced near the plasma periphery than at the centre, and this has the effect of making the experiment particularly sensitive to steep density gradients near the vessel walls.

The positions of the three oblique lines were varied, consistent with the engineering constraints, and minimising the trace T , the optimum configuration was identified as

$\pm\theta$ =	44°	39°	30°
$\mp h$ =	1.19 m	1.04 m	1.00 m.

This configuration is displayed in Figure 4.

(b) The optimisation process used involved twenty smoothing equations, one for each pixel, so values of T, and indeed, of the total usefulness U as well, depended upon the choice of the smoothing parameter β . Figure 5 shows the rms standard deviation of the reconstructed f_j's for the optimum configuration, for an earlier proposal, and for the seven vertical beams alone. The ordinate is normalised so that it gives the factor by which the error in the f_j's exceeds that on the measured quantities I_ℓ. Although the search for the optimum line of sight configuration was performed at the specific value of $\beta = 0.002$, the Figure demonstrates the same configuration is indeed optimum in the sense that T is the best choice for all values of β . These curves also give some guidance as to the best choice of β,

since they show, for example, that for $\beta < 0.001$, the error on the f_j's increases very rapidly.

Figure 6 shows the total usefulness U for the lines of sight for the same configurations. As β becomes vanishingly small U is expected to approach L, the number of lines of sight. That is U approaches 10 when L = 10, and 7 when L = 7 .

The number of resolved pixels as a function of smoothing parameter β is shown in Figure 7 for each of the three line of sight configurations under consideration. When smoothing is virtually absent we find excellent resolution, but at the expense of ridiculously large errors on the f_j's, since the standard deviation is proportional to β^{-1} for small β . On the other hand, if so much smoothing is introduced that the standard deviation falls below unity, then the experimental measurements are being effectively ignored and the resolution reflects this by becoming unacceptably poor. In the case of the optimum JET configuration, we find a resolution of 10 , just equal to the number of lines of sight, when the standard deviation is around two to three, which is about what one might expect.

In the earlier configuration referred to above, the resolution approaches L only when the standard deviation is already as high as 8 . For standard deviation in the region of 2 to 3, the number of resolved pixels is only 8 . This is nevertheless better than the configuration of seven vertical lines of sight alone, when, for the same standard deviation, only six pixels are resolved.

(c) All these calculations have of course been performed for a specific set of pixels, namely, those illustrated in Figure 4. The set of contours to which the pixels conform is determined by a particular choice of the parameters R_1 R_2 R_m and Z_m, which

constitute the JET standard set, for which the values are given in the Appendix. If a set of pixels distributed differently across these same contours had been chosen, then the optimum configuration of lines of sight might well have been different from the one we have identified. If in addition the contour-determining parameters had also been varied, an even more dramatic change in the optimum configuration of lines of sight might have resulted, and this raises the question as to whether the configuration which has been designed to minimise the error for a particular choice of pixels could be used to discriminate between pixel shapes, and so determine the shape of the plasma contours.

To investigate this possibility we generated measurements I_ℓ by simulating a density distribution conforming to JET standard contours. The I_ℓ's were then used to reconstruct the source function using different pixel sets corresponding to different values for the position of R_m. Standard values of R_1 R_2 and Z_m were retained throughout. The sum of the residuals on the I_ℓ's, χ^2, was computed and found to exhibit a well defined minimum at the simulated source function's actual value of R_m, as shown by the open circles in Figure 8.

The error bars attached to the points in this Figure stem from introducing a random error of realistic size (1% of the largest signal) in the data I_ℓ. When reconstruction is performed on a set of pixels that conforms to the correct contours, the value of χ^2 differs from zero only by the average value of this random noise. But if a fit were attempted to the wrong contours, χ^2 would exhibit an additional systematic component reflecting the discrepancy, as well as the noise. Figure 8 shows that this systematic part and the noise are the same size when ΔR_m is as small

as $\pm$ 2 cm, so in this case it appears that the correct contour set can be identified to within a surprisingly narrow margin.

In a second trial, the contours of the simulated density distribution were corrugated, as shown in Figure 9, and so not a member of the family of possible JET shapes. Proceeding as before, f_j's were reconstructed for JET contour sets differing only in their value of R_m. This time the values found for χ^2 proved to be much larger than previously, and although they did display a minimum, it was much less well defined than before (closed circles in Figure 8).

That the values of χ^2 are now large everywhere means that none of the test contour sets bears much resemblance to the simulated contours, but the set for which χ^2 is minimum is the closest approximation that can be found by varying R_m alone. Even so, this best value of R_m is defined to about $\pm$ 4 cm. As the JET contours are defined by four parameters, a complete search would entail minimising χ^2 in four dimensions.

(d) Even in the configuration of lines of sight that we have described as the optimum, not all the lines are equally useful, the values of the usefulness parameter ranging from 18% to 96%. We therefore enquired how many of the ten lines were indeed strictly necessary, and began by removing the least useful, which was the vertical line nearest to the horizontal viewing port. Reconstructio based on the remaining nine lines proved to be virtually indistinguis able from those based on ten, the standard deviation having increased by only 0.3% and the total usefulness of the lines having decreased from 6.99 to 6.97 . We then identified the least useful of the nine lines, whose usefulness was 49%, removed it, and considered reconstructions based on only eight, again producing very little change. This process was repeated until only one line survived,

and the resulting line of sight configurations at the various stages is shown in Figure 10. In Figure 11, we have plotted the total usefulness and the standard deviations characterising the configurations at each stage of the process. It is apparent that the performance of these configurations has begun to deteriorate when seven lines remain.

(e) So far our configurations of sight lines have been optimised for what we have called the standard JET contours, and for twenty pixels distributed in a particular way across these contours (see Appendix). If the pixel distribution across the contours is changed, though without altering the contours themselves, we enquire whether the line of sight configuration is still the optimum.

The original choice of pixels had what would have been equal areas if the pixels had been circles, and we now change to the analogue of equal spacing and recompute reconstructions. We compare the resulting standard deviations with those found originally in the accompanying TABLE, for the earlier, and for our optimum line of sight configurations.

The standard deviations for the early configuration are substantially unchanged by the alteration of the pixel system, meaning that it performs equally well in either system. By contrast, our optimum configuration is 30% more effective in the "equal area" system, but about 30% worse in the "equal spacing" one. So we looked for an alternative optimum configuration in the "equal spacing" pixel system, and found the following set of oblique lines

$\pm\ \theta$	13°	9°	37°	
$\mp\ h$	0	0.5	0.98	metres

and the TABLE indicates that the standard deviation of this

configuration is 8.82 as opposed to the early standard deviation of 4.48 in the system for which the former is optimised. In the equal areas" system, this alternative proves to be marginally superior to the early configuration, but significantly inferior to the optimum previously identified. Its overall performance over the two pixel systems seems to be an improvement on the optimum we had before.

7. Optimising Line-of-Sight Configurations on a Square Array

Hitherto, we have allowed our few lines of sight to be augmented by knowledge of the symmetry of the two dimensional source function whose projections are being measured. We now consider the case where no a priori knowledge of symmetry is assumed. A simple square array of pixels is chosen. The methods already developed are applied to a 3 x 3 square array and used to find the optimum configuration of nine lines of sight.

To begin with, three vertical and three horizontal lines were placed through the pixel centres. The three remaining lines were set at 45° and spaced apart by the same distance as those of the other groups of three, as shown in Figure 12(a). The standard deviation of the resulting reconstruction turned out to be very large compared to the error assumed on the measurements, viz 8.9 times larger. We next optimised the locations of the three oblique lines, holding the vertical and horizontal sets fixed. The result of this exercise was the almost symmetrical pattern shown in Figure 12(b). This time, the standard deviation of the reconstruction was improved to 6.4 , still a very large uncertainty.

Finally we optimised allowing all the lines to vary their positions. The resulting grossly irregular pattern shown in

Figure 12(c) proved to have a standard deviation of only 2.7 , an astonishing improvement on the symmetric pattern of Figure 12(a), which, though it turns out to perform very poorly, is one's intuitive first choice.

That symmetric line-of-sight patterns are often rather poor experimental design can be further illustrated by the following simple example. Suppose all horizontal, vertical, and diagonal lines on a 3x3 square array happened to sum to the same number. Then the underlying distribution might be uniform, as in (a) below, or it could be a "magic square" as in (b). The addition of one more sight line grazing one corner, making nine in all, would still fail to determine the distribution uniquely, since both (b) and its mirror image in a diagonal would satisfy the equations, as indeed, would square (c) too.

(a)			(b)			(c)		
15	15	15	18	3	24	18	11	16
15	15	15	21	15	9	13	15	17
15	15	15	6	27	12	14	19	12

Even if one more line-of-sight were added (now a total of ten) to graze the opposite corner, the data would even then be inadequate. So here it is impossible to deduce the nine elements of a 3x3 square array from data measured on ten symmetrically arranged sight lines. One must resort to an asymmetric configuration to measure even such a simple distribution.

8. Many Lines of Sight

As a final exercise, we increased the number of lines of sight to 30 , disposed in a configuration consisting of six fans of five beams each, as shown in Figure 13. No assumptions about the contours of the source distribution are made, except that it exhibits symmetry about the horizontal plane. We accordingly adopted a square array of independent pixels, 25 in number, bounded by the JET vessel wall.

A simulated source function possessing the contours of the standard JET plasma, and featuring a hollow centre was constructed, and values I_ℓ of observed data on the lines of sight were calculated. From these, the source function was reconstructed, resulting in the distribution shown in Figure 14.

Here, one can see a clearly resolved central minimum, even though the reconstruction standard deviation proves to be very large, namely 10 . To judge the quality of the reconstruction, we compare its contours with those of a standard JET. In particular, the reconstruction mirrors the close packing of JET contours at the outer edge and their wide spacing towards the torus centre.

In view of the suspicion with which we have learned to regard comparatively symmetric arrays of lines of sight during the course of this investigation, we anticipate a considerable improvement could be brought about by optimising the present configuration in the way we have already discussed at length.

9. Conclusions

Conventional matrix inversion has been applied to the problem of recovery of two-dimensional distribution functions from their one-dimensional projections in cases, exemplified by multichannel interferometry, where a few and sometimes only one point at each of a small number of projection angles is measured.

A least squares technique has proved powerful for analysing data expected in such experiments, whose efficiency can be expressed either in terms of the accuracy of reconstruction of the source function, or the freedom from redundancy (usefulness) of the observation channels. Both criteria have been used to optimise the design of experiments, and an optimum design has been shown to increase reconstruction accuracy several fold.

We find that the performance of an asymmetric arrangement of lines of sight is always superior to that of a regular array.

Reconstruction is improved by the judicious application of smoothing. The degree to which smoothing should be applied was investigated in numerical experiments where the effect of smoothing on reconstruction accuracy, on data channel usefulness, and especially on the resolution, were examined. We find that reconstruction error can almost diverge if too little smoothing is used. Our definition of resolution is based on statistical correlations in the source density, and we judge that smoothing should be increased until the natural negative correlation between adjacent pixels just vanishes.

The methods we developed were applied to the ten channel far infrared laser interferometer being prepared for the JET tokamak. Within the engineering constraints, it proved possible to identify an optimum experimental configuration by minimising reconstruction error. We find that contour shape can be identified

rather sensitively if the source density conforms to a contour set which is a member of a predetermined family. It is also possible to determine when the contours are not a member of such a family, even though then, the contours cannot be further defined.

We demonstrate that it is possible to detect contours with no a priori knowledge when more sight lines exist, by recovering a hollow-centred distribution, and reconstructing a recognizable approximation to a set of originally assumed contours, in spite of using a badly designed, i.e. symmetric, configuration of 30 channels and a square array of picture elements.

A FORTRAN programme [13] embodying our techniques for designing experiments and analysing data stemming from them has been prepared.

ACKNOWLEDGEMENT

Our thanks are due to colleagues at the Culham Laboratory, on the JET project, and at Modes Scientific Consultancy Ltd for stimulating discussions.

This work was supported by a JET Design Study Contract.

T A B L E

Line-of-Sight Configuration	Early	Optimum	Alternative
"Equal Area" Pixels	4.26	3.13	4.16
"Equal Spacing" Pixels	4.48	6.01	3.82

Numbers in the TABLE are standard deviations.

REFERENCES

[1] H R Griem Plasma Spectroscopy McGraw-Hill 176-178 (1964)

R Bracewell The Fourier Transform and its Applications McGraw-Hill (1965)

[2] A useful introduction to the subject is
W Swindell and H H Barrett Physics Today 32-41 (Dec 1977)

Two reviews are
A C Kak Proc IEEE 67 1245-1271 (Sept 1979)

T F Budinger and G T Gullberg IEEE Trans Nucl Sci NS-21 2-20 (1974)

[3] G N Hounsfield Brit J Radiology 46 1016-1022 (1973)

[4] R N Bracewell Aust J Phys 9 198-217 (1956)

R N Bracewell and A N Riddle Astrophys J 150 427-434 (1967)

[5] N R Sauthoff and S von Goeler IEEE Trans in Plasma Sci PS-7 141-147 (1979)

B R Myers and M A Levine Rev Sci Instr 49 610-616 (1978)

[6] J Radon Der Sachsische Akademie der Wissenschaften 29 262-277 (1917)

[7] A M Cormack J Appl Phys 34 2722-2727 (1963)

A M Cormack J Appl Phys 35 2908-2913 (1964)

[8] J H Williamson and M E Clarke J Plasma Phys 6 211-221 (1971)

[9] M V Berry and D F Gibbs Proc Roy Soc A314 143-152 (1970)

F M Larkin B I T 9 30-52 (1969)

N H Olsen, C D Maldonado, and G D Duckworth J Quant Spect Rad Trans 8 1419-1430 (1968)

D J DeRosier and P B Moore J Mol Biol 52 355-369 (1970)

Shi-Kuo Chang and C K Chow IEEE Trans on Computers C-22 18-28 (1973)

A J Hamonic Culham Report CLM P-526 (1978)

[10] D Veron Infrared and Submillimeter Waves Vol II Chap 2 69-135 Academic Press Inc (1979)

[11] P G Guest Numerical Methods of Curve Fitting Cambridge University Press (1961)

[12] B J Green and H P Zehrfeld Nucl Fusion 17 1133-1141 (1977)

[13] J H Williamson JETCAT: A Programme for Computerised Tomography Culham Report CLM R-210 (1982)

[14] D W Sweeney and C M Vest Appl Optics 11 205-207 (1972)

[15] G Frieder and G T Herman J Theor Biol 33 189-211 (1971)

APPENDIX

Calculation of the transfer matrix A

The nested pixels are defined by a function $\Psi(x,y)$ which varies from zero at a point within the plasma to unity at its edge. For sources with circular symmetry, Ψ would be just x^2+y^2, and for JET, Ψ is given by [12]

$$\Psi = (\xi/\xi_2)^2 + (\eta/\eta_m)^2 \frac{\xi_2^2 - 2\xi\,\xi_m + \xi_m^2}{\xi_2^2} \qquad \ldots(A1)$$

where $\xi \equiv R^2 - R_o^2 = x(x+2R_o)$

$\xi_m \equiv R_m^2 - R_o^2 = x_m(x_m+2R_o)$

$\xi_2 \equiv R_2^2 - R_o^2 = x_2(x_2+2R_o)$

$\eta_m \equiv z_m = y_m$

$\eta \equiv z = y$

$$R_o^2 = \tfrac{1}{2}(R_1^2 + R_2^2) .$$

For JET, $R_o = 3.213$ metres

$R_1 = 1.71$ "

$R_2 = 4.21$ "

$R_m = 2.61$ "

$z_m = 2.10$ " .

Both these choices for Ψ give pixels of roughly equal area, but the spacings can be varied, for instance to equal steps in radius by replacing Ψ by $\sqrt{\Psi}$, or to closer spacing near the edge by substituting Ψ^2. The centre line of pixel j is defined as the contour $\Psi = (j-1)/J$, so that the $(J+1)$th pixel (at which the distribution equals zero) would be centred on the plasma boundary.

At a point between the pixel centre lines j and j+1, the source intensity is obtained by interpolating between f_j and f_{j+1}. Spline fitting was not used because its "action at a distance" would allow a measurement in the outer region to imply something about the intensity in the (possibly unobserved) interior. In order to deal logically with the region near the origin (pixel 1), the interpolation was made linear in ψ^2 rather than in ψ :

$$f(\psi) = f_j + (f_{j+1} - f_j) \frac{\psi^2 - \psi_j^2}{\psi_{j+1}^2 - \psi_j^2} \quad . \qquad \ldots(A2)$$

Each row in matrix A is obtained by integrating along the line-of-sight, each step contributing to two elements $A_{\ell j}$ and $A_{\ell j+1}$ according to the proportions indicated by equation (A2), i.e.

$$A_{\ell j} = \int g[\psi(x,y),\ j]\ ds \quad . \qquad \ldots(A3)$$

where
$$g[\psi, j] = \begin{cases} \dfrac{J^2\psi^2 - (j-2)^2}{2j-3} & \text{for } j-2 \le J\psi \le j-1 \\ \dfrac{j^2 - J^2\psi^2}{2j-1} & \text{for } j-1 \le J\psi \le j \\ 0 & \text{for } J\psi > j \text{ or } J\psi < j-2 \end{cases} \qquad \ldots(A4)$$

When a rectangular mesh of pixels is used, the simplest procedure is to evaluate the length of the line-of-sight in each (constant density) pixel. Once again, a smoother result can be obtained by interpolation. The source function is taken to be f_j at mesh point j and the density between pixels is calculated by bilinear interpolation. Working relative to the centre of one pixel in units of the mesh interval, its influence at point (x,y) is $(1-|x|)(1-|y|)$ out as far as the next row and

column of the mesh, $x = \pm 1$, $y = \pm 1$, beyond which its influence is zero.

The calculation of matrix A proceeds by splitting the line-of-sight into segments obtained by cutting along the rows and columns of the mesh. Each segment gives a contribution to each of the elements in A corresponding to the four pixels that surround it. To avoid problems with lines-of-sight that are almost parallel to the x and y axes, the integration is performed with respect to s, the distance along the line. The perpendicular distance from the centre of the pixel to the line is p , and s is measured from this perpendicular. Contributions to $A_{\ell j}$ of the form

$$\int_{s_1}^{s_2} (1-|x|)(1-|y|)\, ds =$$

$$\Big\{ s + \text{sign}(x)[sp\,\sin\theta - \tfrac{1}{2}s^2\cos\theta] - \text{sign}(y)[sp\,\cos\theta + \tfrac{1}{2}s^2\sin\theta] - \text{sign}(xy)[[\tfrac{1}{2}sp^2 - s^3/6]\,\sin 2\theta - \tfrac{1}{2}s^2 p\,\cos 2\theta] \Big\}_{s_1}^{s_2} \qquad \ldots(A5)$$

are summed for every segment that the line produces.

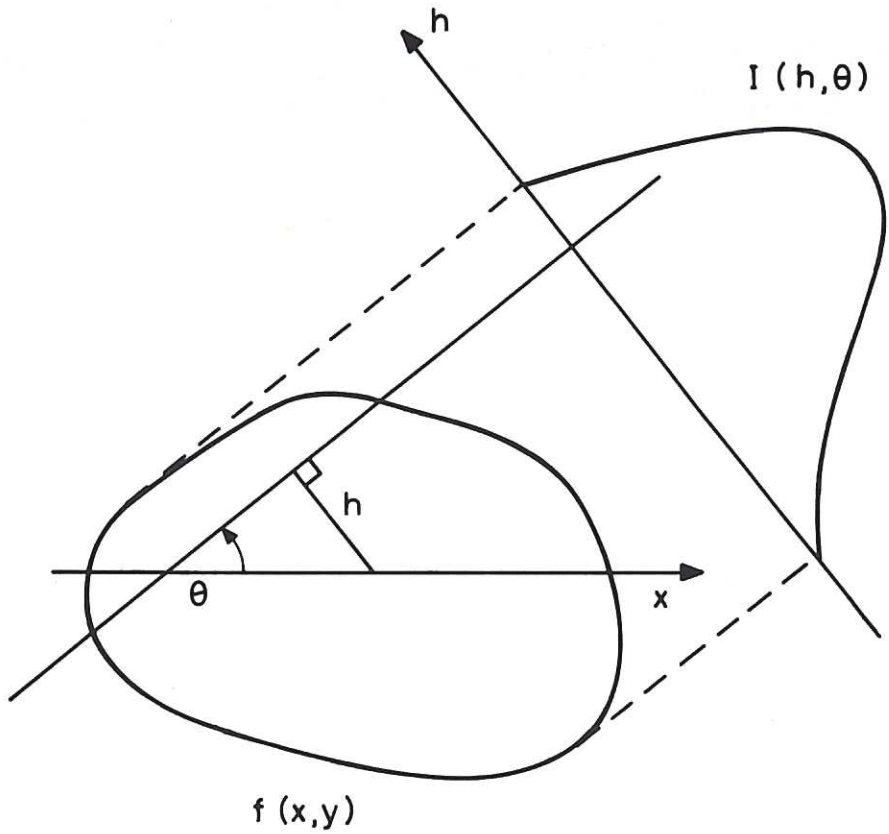

Fig.1 The two-dimensional distribution f(x,y), whose one-dimensional projection in the direction θ, I(θ, h), is measured. The problem is to reconstitute f(x,y) given some values of I (θ, h).

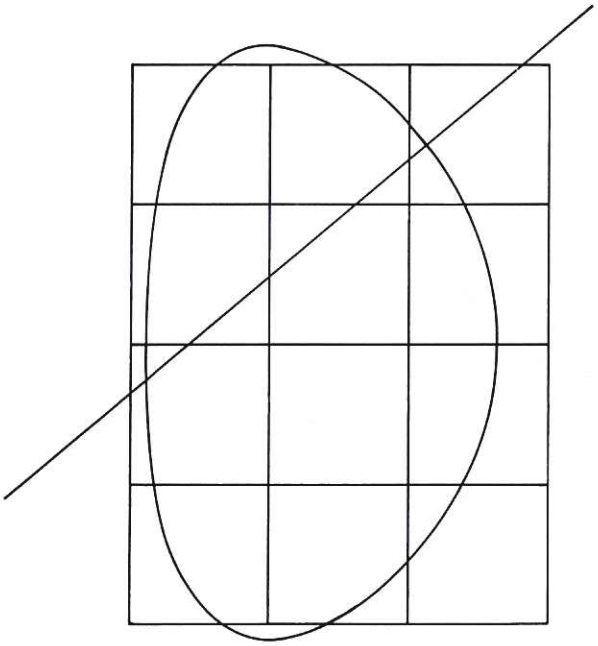

Fig.2(a) An arbitrarily chosen array of square picture elements (pixels) superimposed on the plasma cross-section.

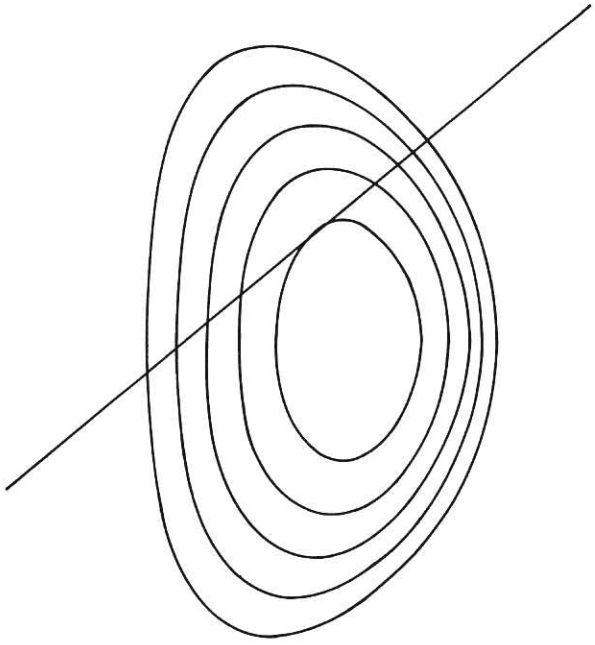

Fig.2(b) A set of pixels bounded by magnetic surface contours.

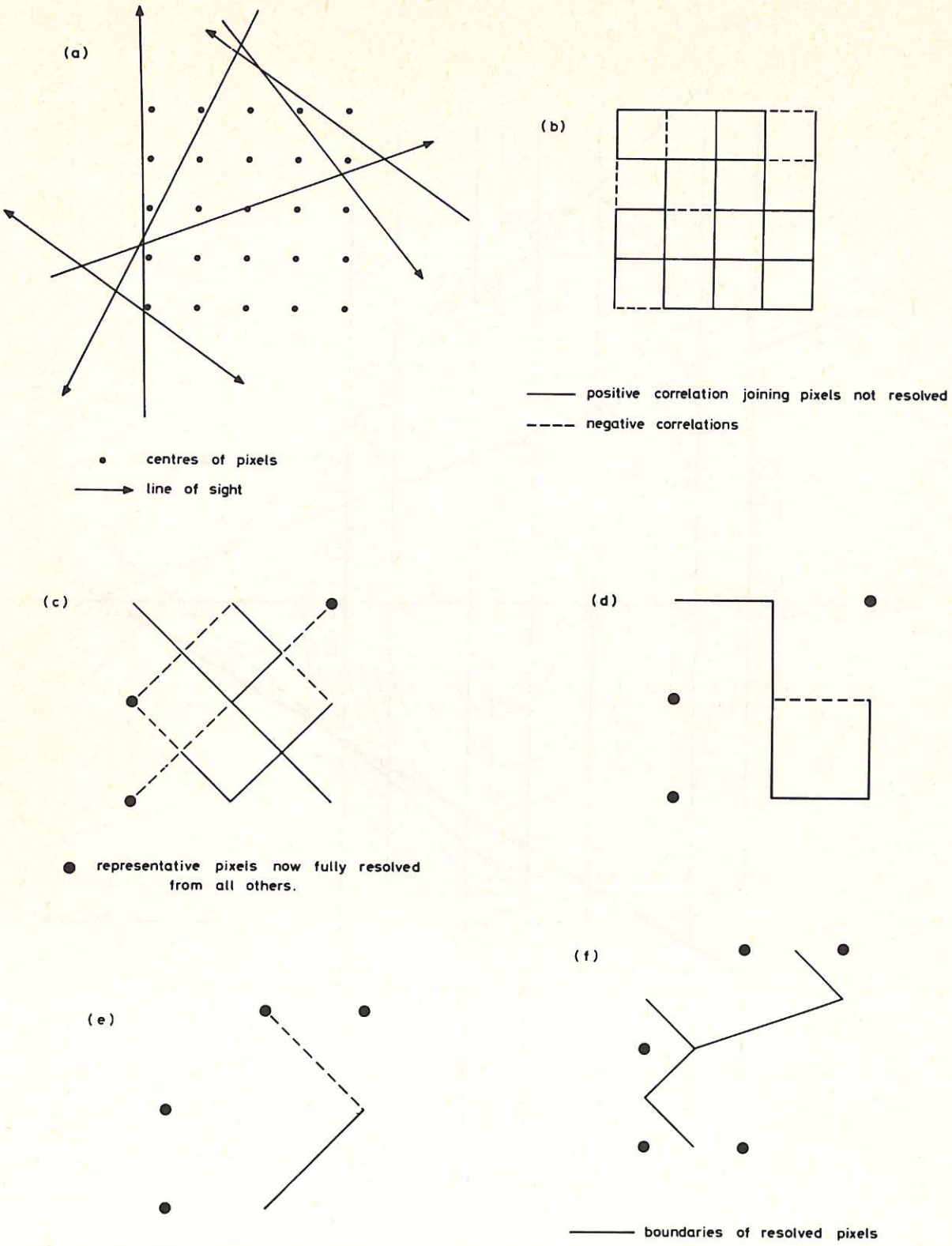

Fig.3 Determining resolution on a square array of twenty five pixels traversed by six randomly located lines-of-sight. (a) shows the arrangement under investigation; (b) to (e) solid lines denote positive correlations, dashed lines negative ones. (f) Lines serve to delineate roughly the boundaries of the resolved regions. See text for a detailed explanation.

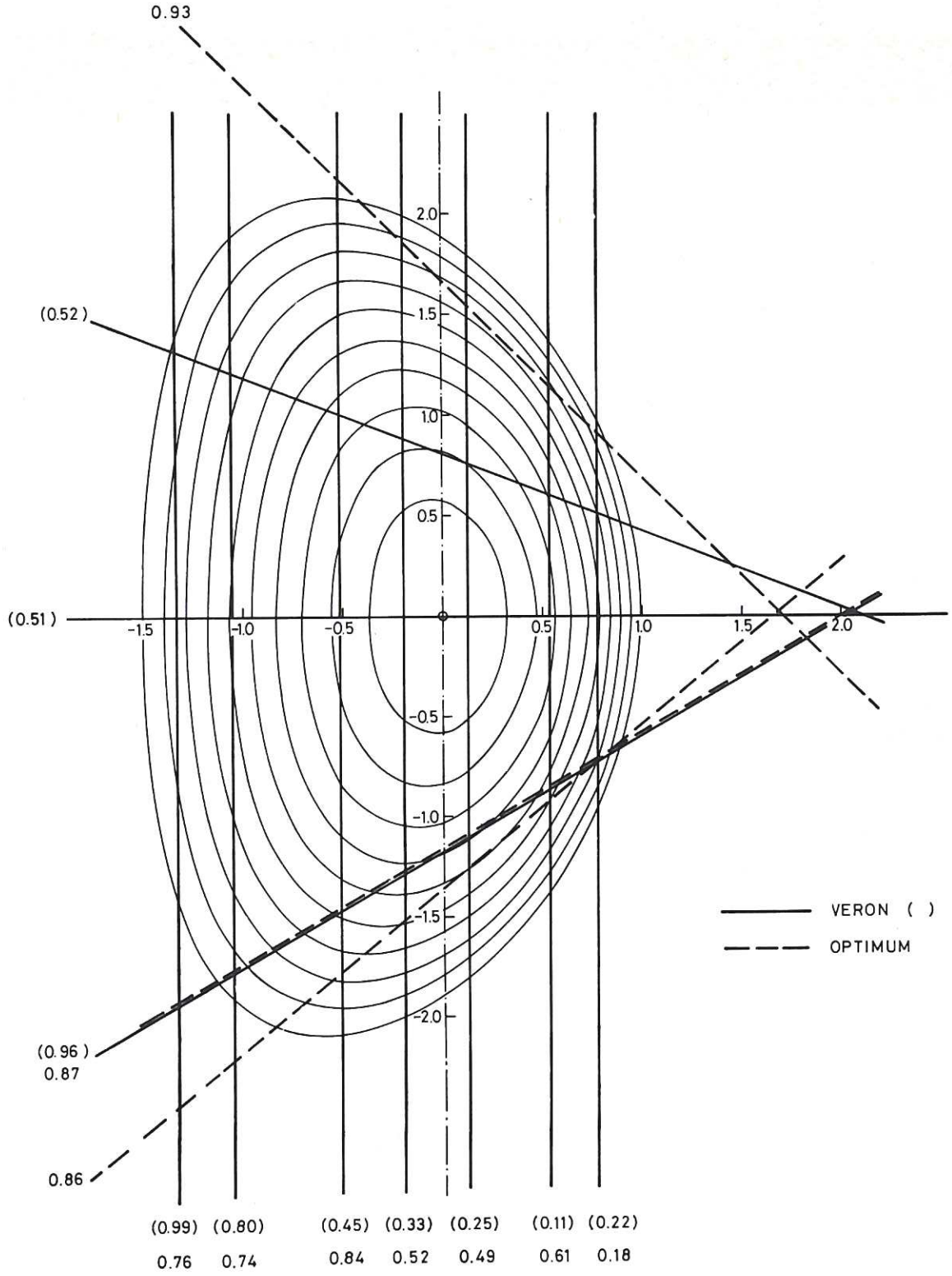

Fig.4 Set of nested magnetic contour lines defining the JET standard set of pixels. The ten straight lines are the proposed FIR laser interferometer channels. Dashed lines are an alternative, superior, subset; vertical lines are common to both 'earlier' and 'superior' configurations. The number attached to each sight line is its 'usefulness' in its configuration. Numbers in brackets ( ) refer to the 'earlier' configuration.

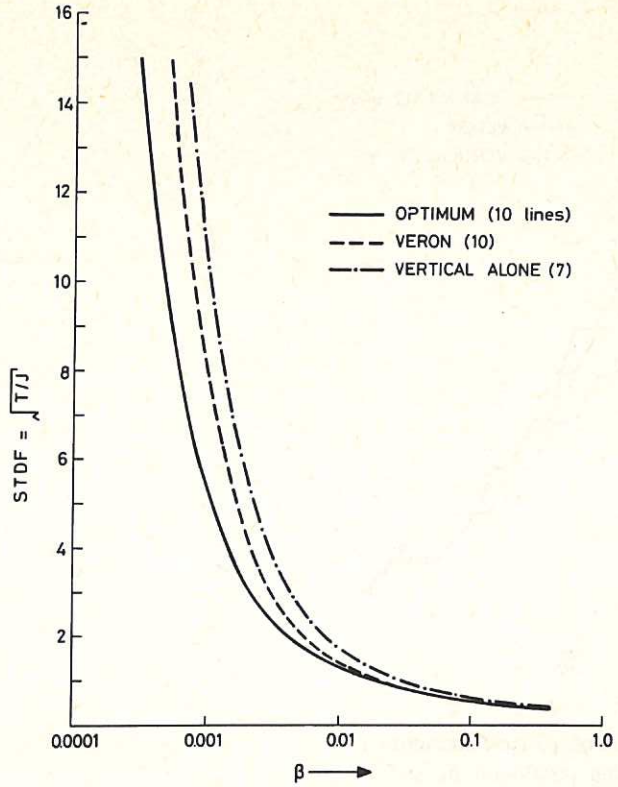

Fig.5 Error (rms standard deviation) of the reconstructed f_j's for the optimum configuration (——), the earlier proposal (– – –), and the seven vertical lines-of-sight alone (–·–·–), as functions of smoothing parameter β defined in the text.

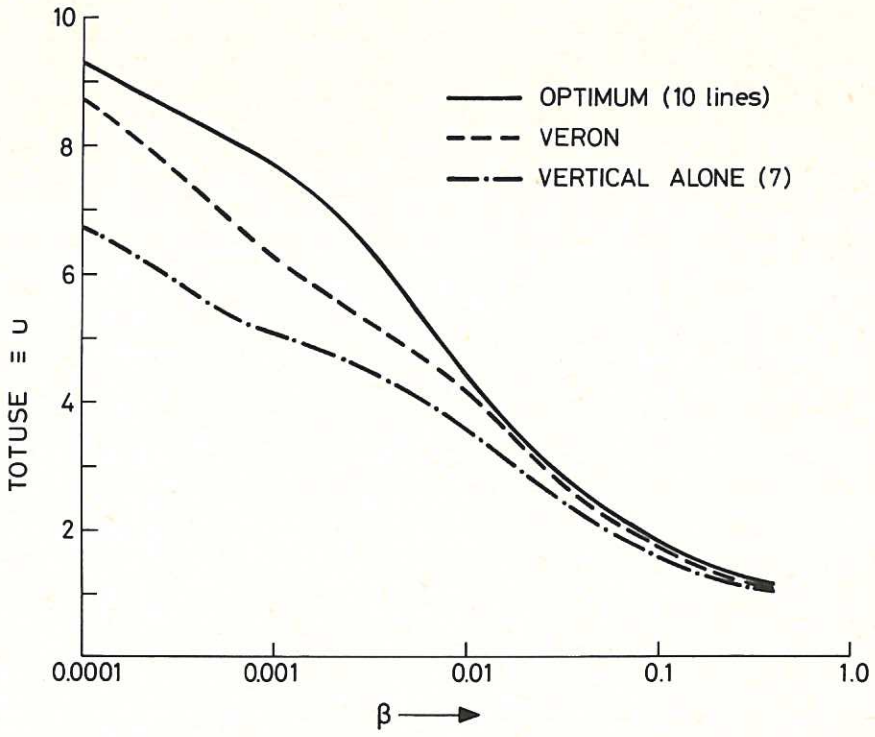

Fig.6 The total usefulness U for the optimum configuration of ten channels (——), the earlier proposal for ten channels (– – –), and seven vertical channels alone (–·–·–) as functions of smoothing parameter β.

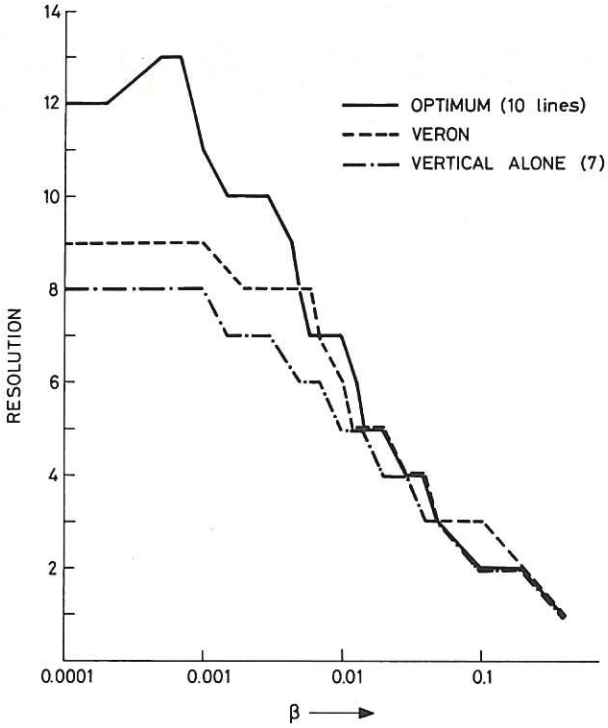

Fig.7 Number of resolved picture elements as a function of smoothing parameter β, for the optimum configuration (———), for the earlier proposal (– – –), and for seven vertical channels alone (–·–·–).

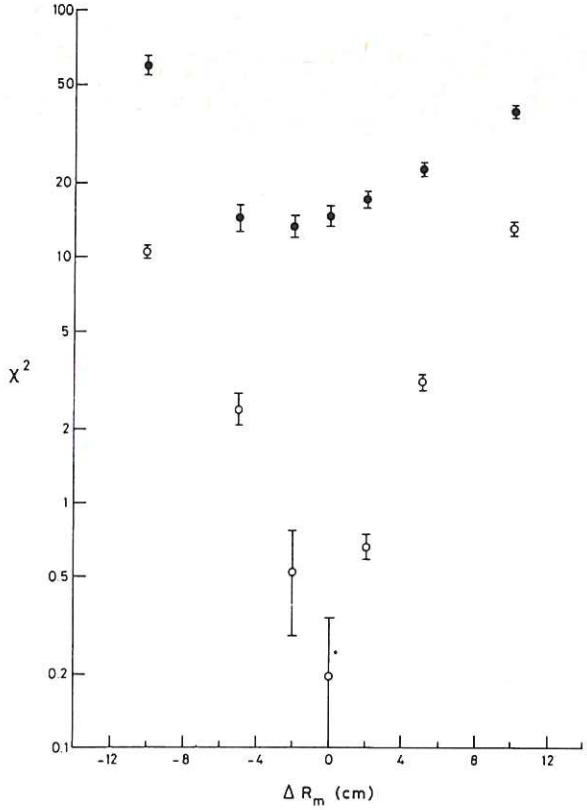

Fig.8 Discriminating contour shapes. Open circles when simulated distribution conforms to one of the possible JET configurations, closed circles when it does not.

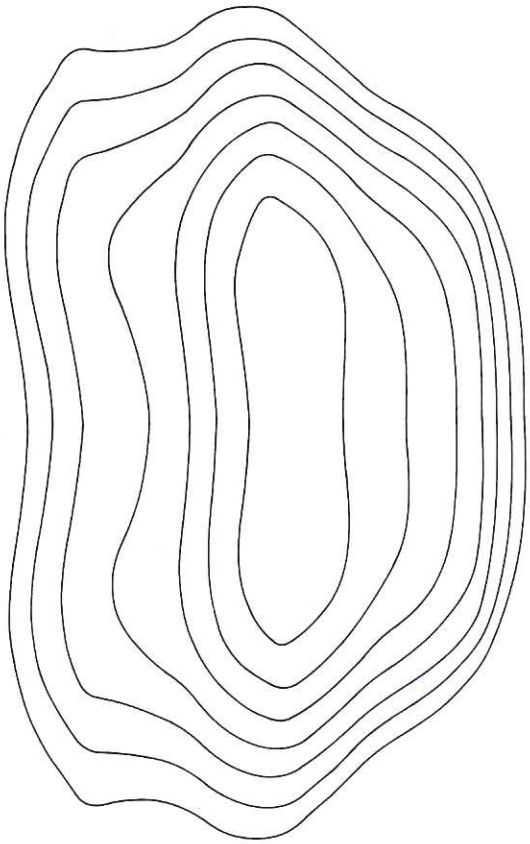

Fig.9 Corrugated contours of simulated density distribution giving χ^2 shown by closed circles in Fig.8.

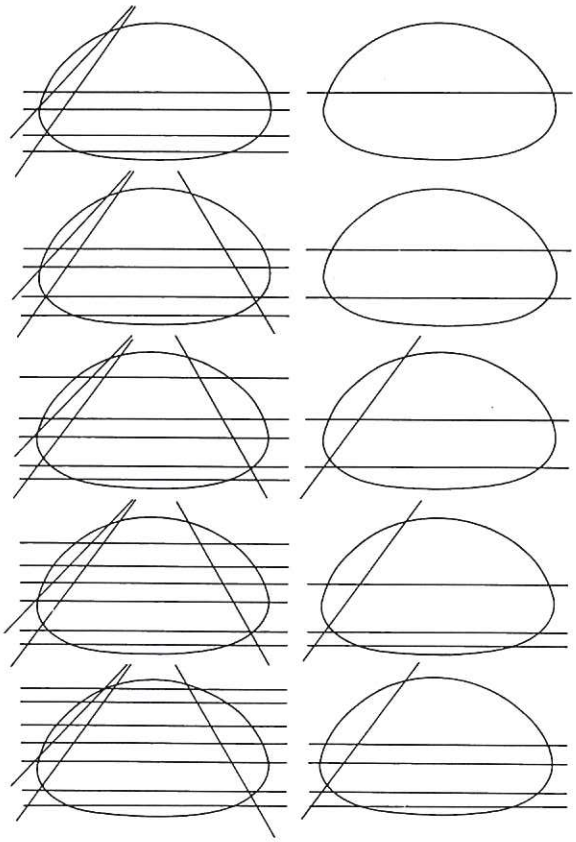

Fig.10 Sequential elimination of least useful line from optimum configuration. After removing least useful line, usefulness of remaining lines is recalculated, and the least useful is again removed, and so on.

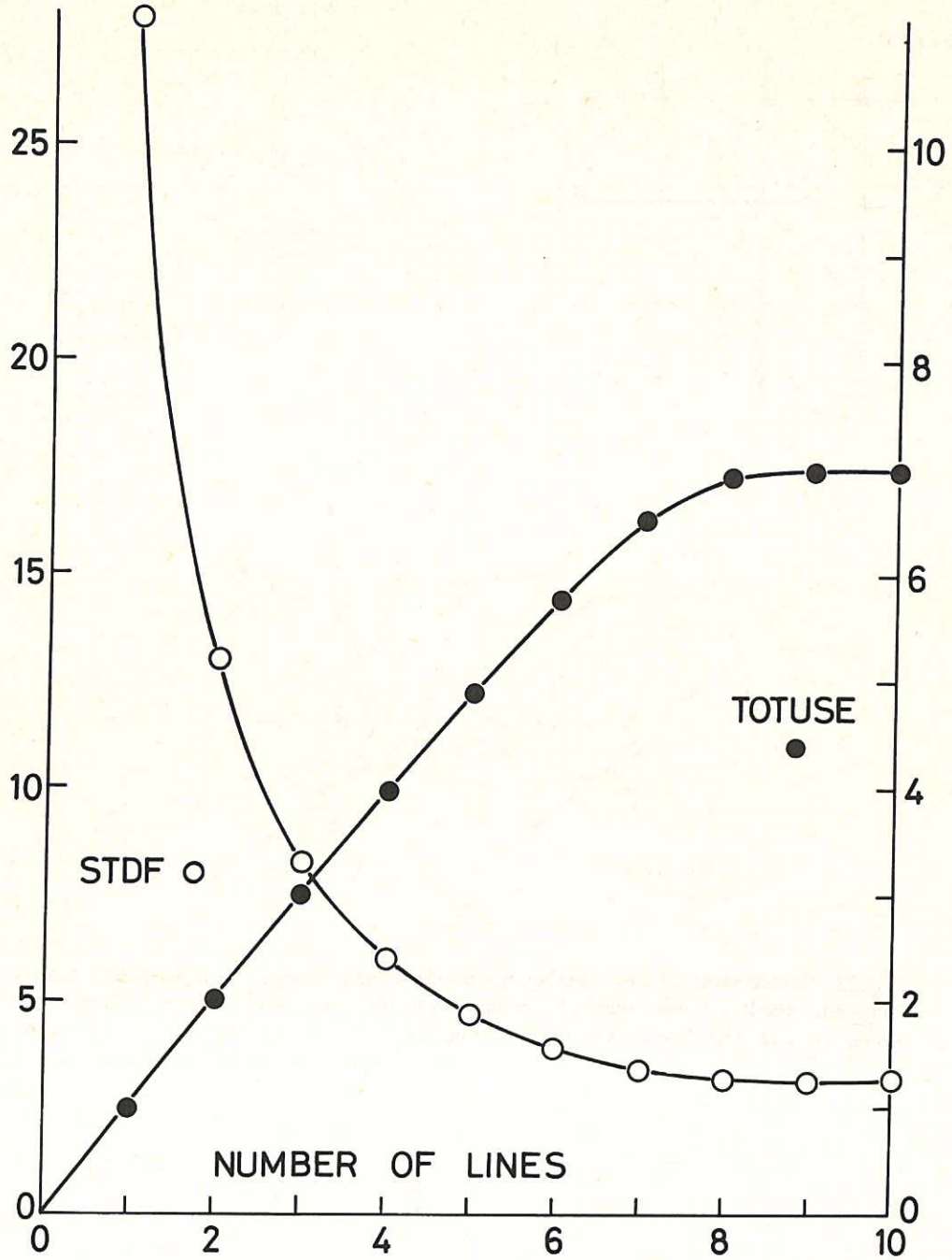

Fig.11 Total usefulness of lines (right hand scale) and standard deviation (left hand scale) of reconstruction based on remaining lines at each stage of the process illustrated in Figure 10.

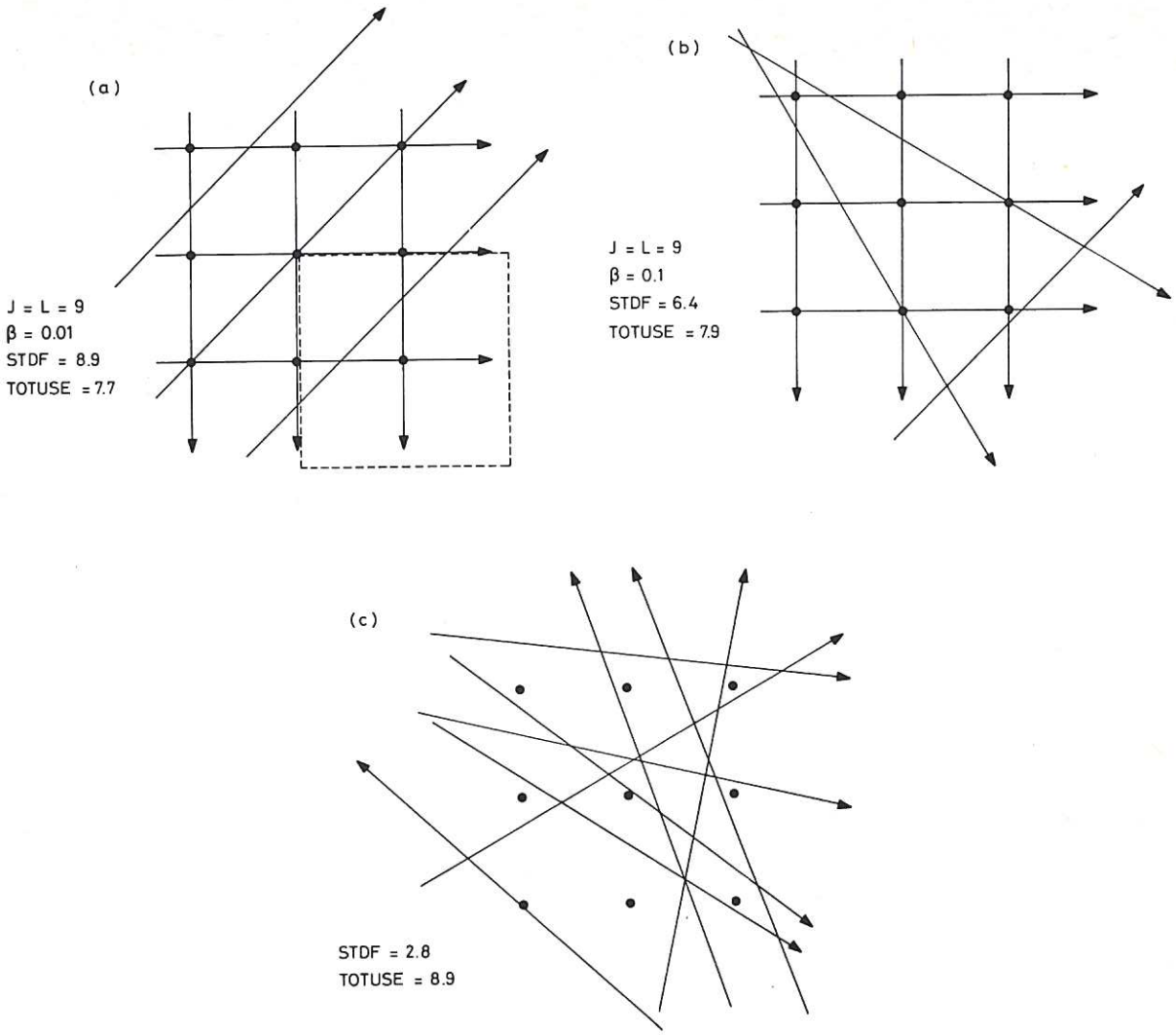

Fig.12 Square array of nine overlapping pixels (centres marked by dots; dashed lines show one pixel) with nine regularly arranged sight lines. Reconstruction error improves as sight line configuration becomes more random.

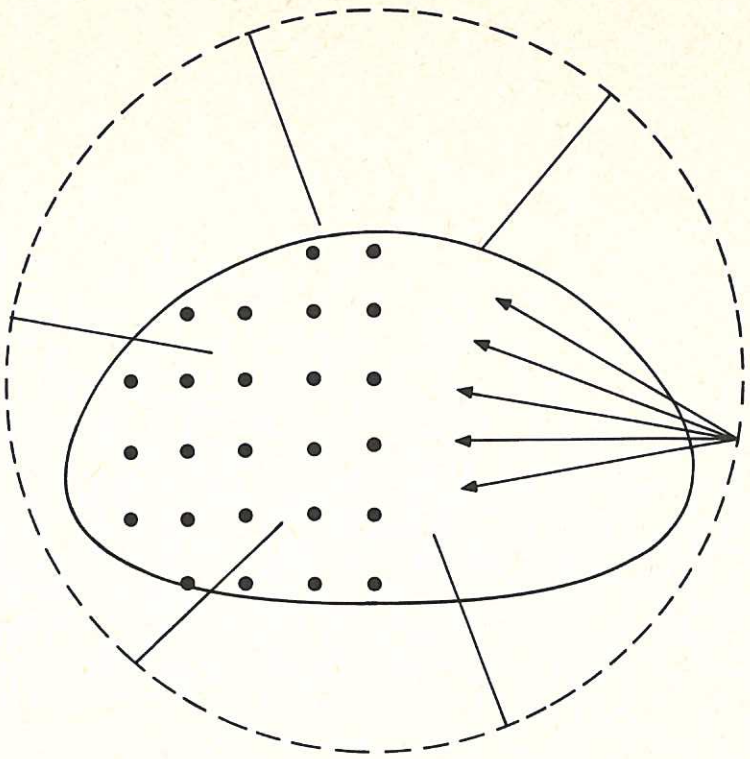

Fig.13 Regular array of square pixels and symmetric configuration of thirty sight lines used to attempt reconstruction of simulated hollow centre density profile, when no contours are assumed.

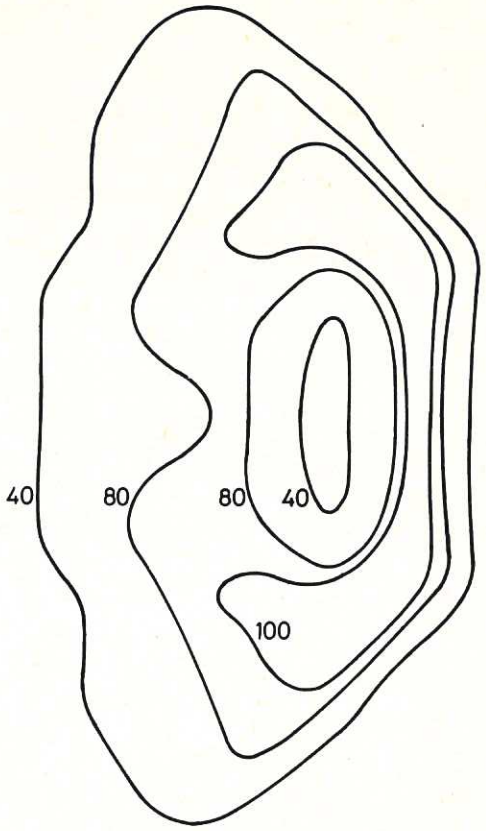

Fig.14 Reconstructed distribution using arrangement shown in previous Figure. Lines of constant density (relative density indicated by attached number) deduced from simulated data.